Supporting Information

Materials and Reagents: Poly(allylamine hydrochloride) (PAH), N-Hydroxysuccinimide (NHS) and 1-(3-Dimethylaminopropyl)-3-ethylcarbodiimide (EDC), 4',6-diamidino-2-phenylindole (DAPI) were purchased from Sigma-Aldrich. Dimethylsulfoxide (DMSO) and ethanol (C_2H_5OH) were purchased from Tianjin Fengchuan Chemical Reagent Technologies Co., Ltd. All chemicals were used without further purification and all the solvents used were of analytical grade. RPMI-1640 and DPBS (no calcium, no magnesium) were purchased from Mediatech, Inc. Trypsin-EDTA solution was purchased from Beijing Solarbio Science & Technology Co., Ltd. Fetal Bovine Serum (FBS) was purchased from Zhejiang Tianhang Biotechnology Co., Ltd. Cell culture flasks, cell culture plates and cell culture dishes were purchased from Nest Biotechnology Co., Ltd. ActinRed™ 555 ReadyProbes® Reagent was purchased from Thermo Scientific. Anti-actin mouse monoclonal antibody was purchased from Sangon Biotech (Shanghai) Co., Ltd. HeLa and NG108-15 cells were obtained from the China Center for Type Culture Collection (Wuhan, P.R. China) and cultured at 37 ℃ with 5% CO_2 in Complete Medium (CM) (consisting of RPMI-1640 medium supplemented with 10% FBS and 1% penicillin-streptomycin). Deionized water from a Milli-Q IQ 7000 Ultrapure Water system (18.2 MΩ; Millipore, Molsheim, France) was used throughout this study.

Instrumentations: ESI-TOF-MS spectroscopy of Au_{10}NCs in ethanol was conducted using an AB SciexX500R Q-TOF spectrometer. Fourier transform infrared (FT-IR)

spectroscopy was conducted using a Bruker TENSOR 27 FT-IR spectrometer in the 500-4000 cm^{-1} region with KBr pellet method. TEM images were acquired with a Tecnai G2 F20 S-TWIN transmission electron microscope (operated at an acceleration voltage of 200 kV). Dynamic light scattering (DLS) measurements were performed on a Horiba SZ-100 Nanoparticle Size Analyzer. UV-visible absorption spectra were recorded on a TU-1901 double-beam UV-Vis spectrophotometer. Steady-state excitation and emission spectra of the compounds were analyzed using a Horiba FluoroLog-3 spectro fluorometer. Luminescence lifetime was analyzed using an Edinburgh FLS980 fluorescence spectrometer equipped with a 355 nm laser operating in time-correlated single-photon counting mode (TCSPC) with are solution time of 200 ps. The luminescent quantum efficiency of Au_{10}NCs was analyzed using an integrating sphere at excitation wavelength of 371 nm via Edinburgh FLS980 fluorescence spectrometer. Confocal imaging was performed with a Leica TCS SP8 confocal fluorescence microscope.

X-Ray crystallography: Single-crystal X-ray diffraction (SCXRD) measurements were performed on a Rigaku XtaLAB Pro diffractometer with Mo-Kα radiation (λ = 0.71073 Å) at 150 K. Data collection and reduction were performed using the program CrysAlisPro.[1] Crystal data for Au_{10}NCs, orthorhombic, $P2_12_12$, a = 19.6562(4) Å, b = 28.6975(5) Å, c = 21.2232(4) Å, α = β = γ = 90 °, V = 11971.7(4) Å3, Z = 2, 319546 reflections collected, 30031 unique (R_{int} = 0.1049), final R_1 = 0.0460, wR_2 = 0.1064 for 30031 observed reflections [I>=2σ (I)]. All the structures were solved with direct methods (SHELXS)[2] and refined by full-matrix least squares

on F^2 using OLEX2,[3] which utilizes the SHELXL-2015 module.[4] All the atoms were refined anisotropically with the exception of some solvent molecules. Detailed information regarding the crystal data, data collection and refinement results for Au_{10}NCs are provided in Table S1-S3.

Synthesis of Au_{10}NC: Au_8NC was prepared according to a previously reported study by our group.[15] Levonorgestrel solution (2 mL, 25 μM, DCM/CH_3CN = 1:1) was added in one portion followed by neat NEt_3 (8 μL). Me_2SAuCl (7.4 mg) was then added under stirring to yield a green transparent solution, then stirred for 5 min and allowed to evaporate slowly in the dark at room temperature to yield yellow block crystals (Au_8NC). Au_8NC (10 mg) crystals was dissolved in DMSO (3 mL) in an oven at 45 ℃ for one month to obtain Au_{10}NC. CCDC number: 1995917.

Fabrication of Au_{10}NC-PAH-Ab: Aqueous PAH solution of different concentration was added to Au_{10}NC (5 μM) solution under continuous stirring for 60 min to prepare Au_{10}NC-PAH assemblies. The mixture consisting of 1-(3-Dimethylaminopropyl)-3-ethylcarbodiimide (EDC, 0.5 mM), N-Hydroxysuccinimide (NHS, 0.05 mM) and anti-actin antibodies (10 μM) was shaken for six hours gently to activate them. Then, an equal volume of Au_{10}NC-PAH (containing 5 μM Au_{10}NC and 0.2 μM PAH) assemblies were added to the mixture and shook for four hours continuously. Then, Au_{10}NC-PAH-Ab was centrifuged at 5000 r/min for 10 min. The antibody concentration in supernatant was analysed by BCA Protein Assay Kit to be 51.8 μg/mL. Conjugated efficiency = mass of

conjugated Ab/total mass of Ab = 75.6%. FT-IR spectra in Fig. S17 shown that the spectrum of Au_{10}NC-PAH-Ab displayed both characteristic peaks of alkynyl at 1976 nm and amide bond (amine N-H stretch at 3293 nm, C=O stretch at 1650 nm, N-H bending at 1532 nm), indicating a successful conjugation.

Cytotoxic assays: NG108-15 cells were planted into 96-well plate (2×10^4 cells per well) and grown overnight with RPMI-1640 containing with 10% FBS at 37 ℃, 5% CO_2. After cell attachment, 100 μL fresh medium supplemented with different concentrations of Au_{10}NC-PAH-Ab (1, 2, 5, 10, 20, 30 μM) were added to per well, respectively. 24 h later, 10 μL CCK-8 was added to each well for 1 h incubation. Absorbance of each well at 450 nm was determined on an EnSight™ Multimode Plate Reader. Relative cell viability (%) was calculated as $(A_{test}/A_{control}) \times 100$. The IC_{50} and IC_{10} was calculated using CompuSyn software.

Cell imaging: HeLa and NG108-15 cells were cultured for 12 h on glass-bottomed Petri dishes with an initial density of 2×10^4 cells/dish. The medium was then replaced with cell medium containing Au_{10}NC-PAH-Ab (2 μM) and cultured for 24 h. Then, cells were washed with DPBS for 3 times, fixed with paraformaldehyde (4%) for 10 min, treated with Triton X-100 (0.25%) for 10 min, and incubated with bovine serum albumin (1.2%) for 2 h at 37 ℃. To evaluate the labeling effect of Au_{10}NC-PAH-Ab, ActinRed™ 555 ReadyProbes™ Reagent (diluted 10-fold in DPBS) was added for 30 min at room temperature and rinsed with DPBS. To stain nucleus, cells were incubated with DAPI (50 μg/mL in DPBS) for 15 min and washed with

DPBS for three times. Confocal images of the cells were acquired with a Leica TCS SP8 confocal fluorescence microscope (excitation wavelength: 405 nm, 552 nm).

RA-induced cell differentiation: NG108-15 cells were seeded on glass-bottomed Petri dishes with an initial density of 1×10^4 cells/dish. Aqueous PAH solution (to a final concentration of 0.2 μM) and RA (to a final concentration of 10 μM) was added to Au_{10}NC (5 μM, 5 mL) solution under continuous stirring for 60 min to prepare RA loaded Au_{10}NC-PAH assemblies. The solution was then centrifuged to separate unloaded RA followed by HPLC measurement of supernatant at 340 nm for RA quantification, with reference to a standard calibration curve. Loading content = (total mass of RA – mass of supernatant RA)/mass of Au_{10}NC-PAH-RA. Entrapment efficiency = (weight of RA in Au_{10}NC-PAH-RA)/(initial weight of RA). The RA loading content of Au_{10}NC-PAH-RA (with a RA concentration of 1.31 μg/mL, equal to 4.36 μM) was calculated to be 4.3%, and the entrapment efficiency was calculated to be 43.6%. After the cells were allowed to adhere to the substrates, RA and RA loaded Au_{10}NC-PAH assemblies was added to the cell medium respectively to a final RA concentration of 1 μM, and cultured for 7 days.

For cell type, we incubated HeLa cells with free RA and Au_{10}NC-PAH-RA (1 μM RA equivalent concentration, containing 1.15 μM Au_{10}NCs) for 48 h, 3 days and 7 days as control experiments. As shown in Fig. S24-25, there is no neurite outgrowth observed. We added neurite outgrowth situations about NG108-15 cells of blank group and groups incubated with Au_{10}NC-PAH, free RA for different time as shown in Fig. S26-28. We also incubated NG108-15 cells with a lower concentration of

Au_{10}NC-PAH-RA (0.5 μM RA equivalent concentration) for different time. As shown in Fig. S29, neurite lengths of this group are shorter than high concentration group in Fig. 5 and Fig. S30.

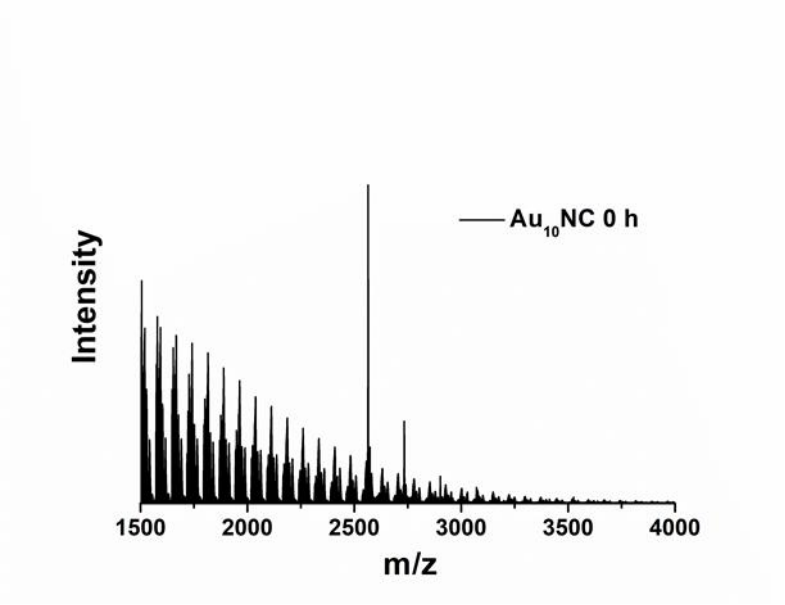

Fig. S1 ESI-TOF-MS spectra of Au_{10}NC dissolved in CH_2Cl_2/CH_3CN at 0 h.

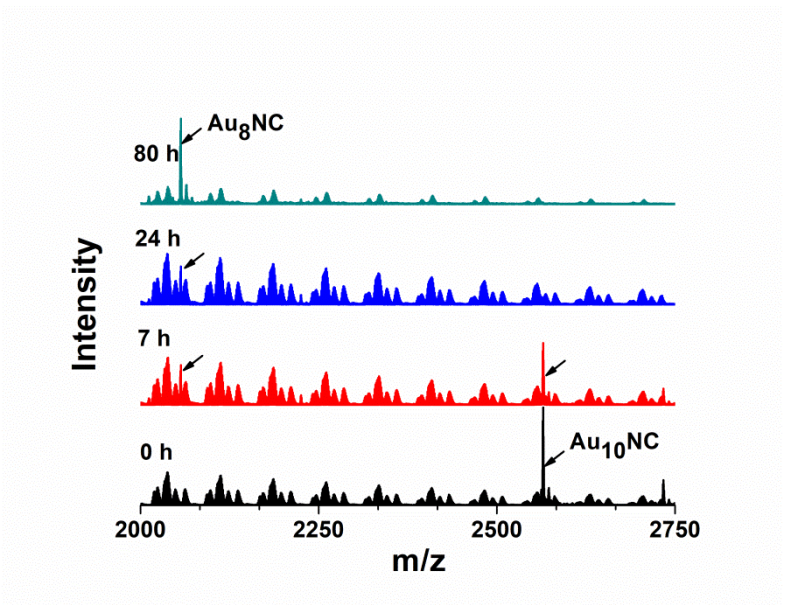

Fig. S2 ESI-TOF-MS spectra of Au_{10}NC dissolved in CH_2Cl_2/CH_3CN for different time.

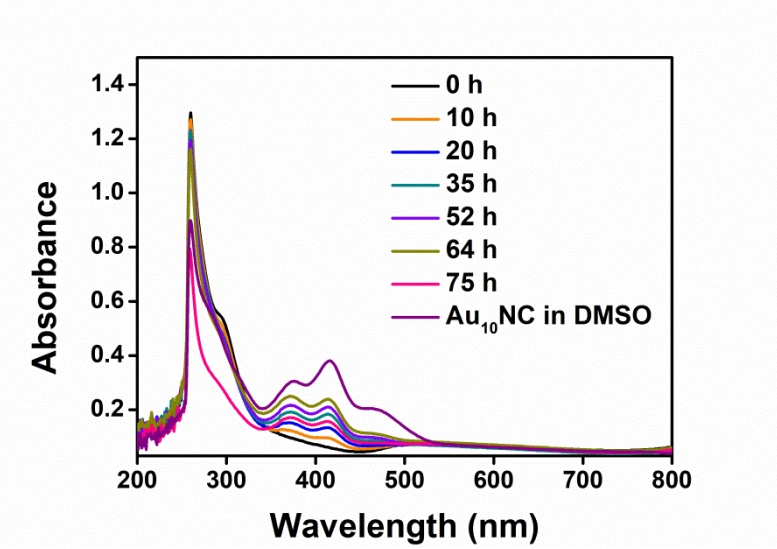

Fig. S3 UV-Vis spectra of Au_8NC dissolved in DMSO for different time (converted to Au_{10}NC).

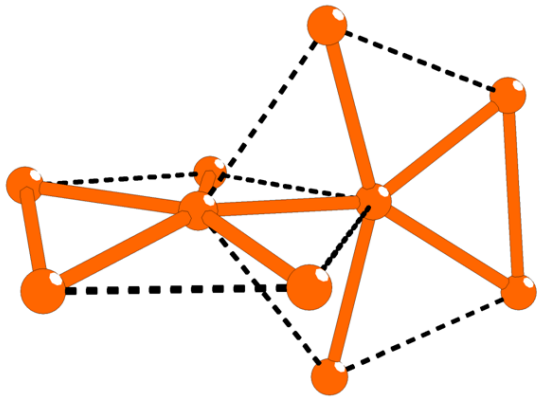

Fig. S4 The near-planar pentagonal structure of Au_{10}NC inner core.

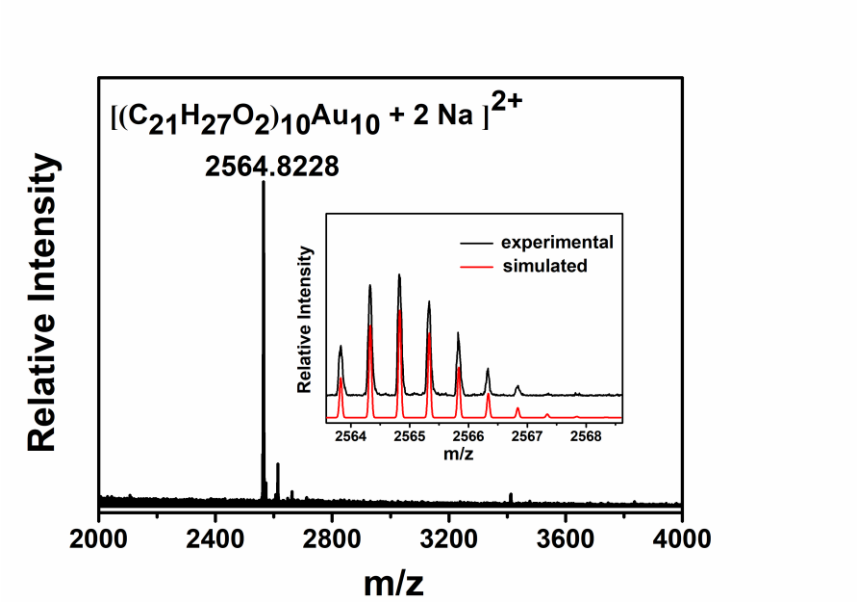

Fig. S5 Positive mode ESI-TOF-MS spectrum of the Au_{10}NCs. The inset shows an enlarged portion of the spectrum showing the measured (black line) and calculated (red line) isotopic distribution patterns.

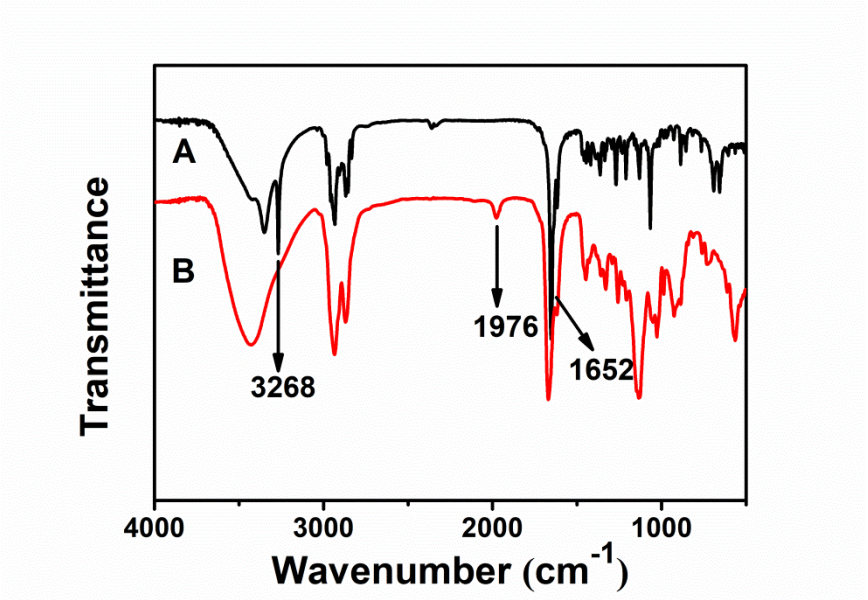

Fig. S6 The FT-IR spectra of the levonorgestrel ligand (A) and Au_{10}NCs (B).

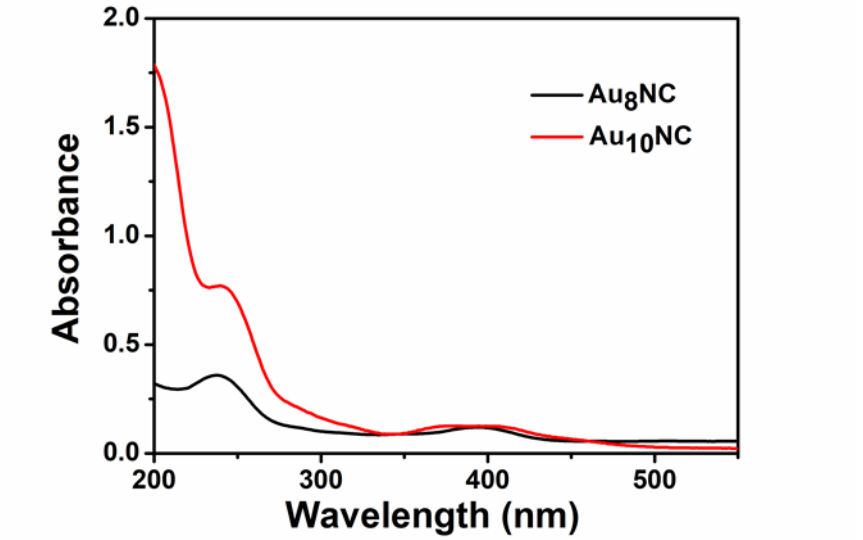

Fig. S7 UV-Vis spectra of Au_{10}NCs (red line) and Au_8NCs (black line).

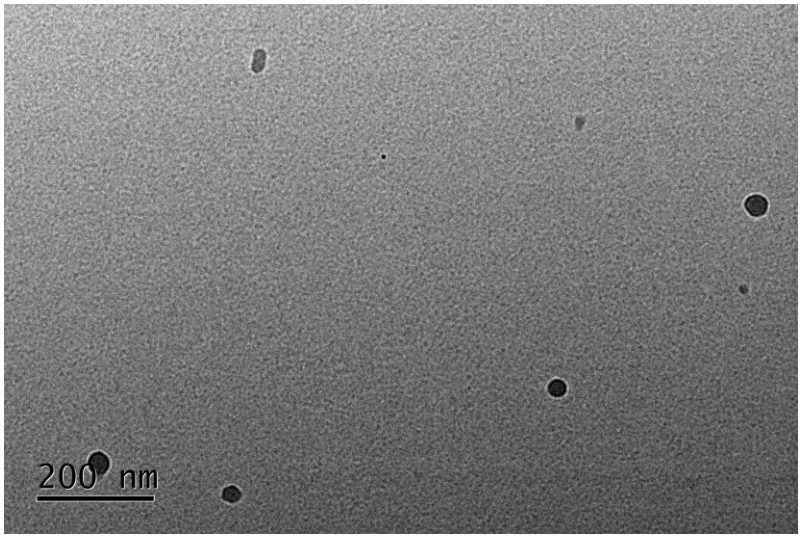

Fig. S8 TEM image of Au_{10}NC-PAH (0.1 μM).

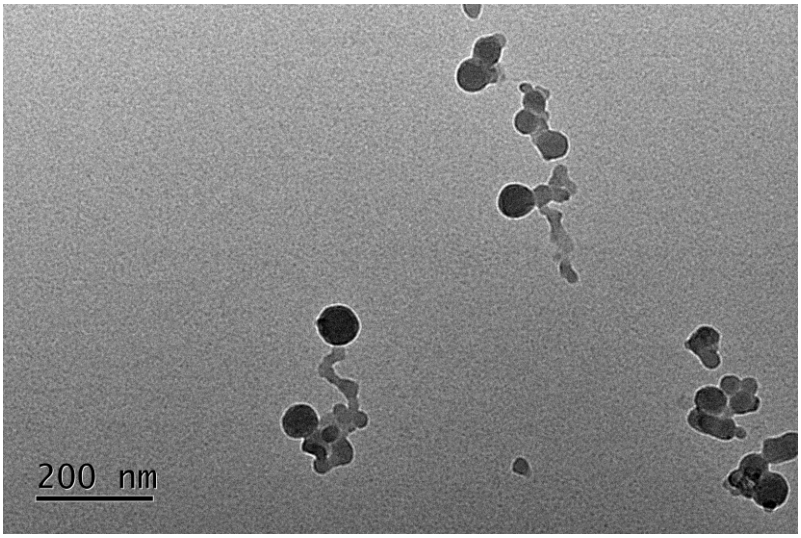

Fig. S9 TEM image of Au_{10}NC-PAH (0.8 μM).

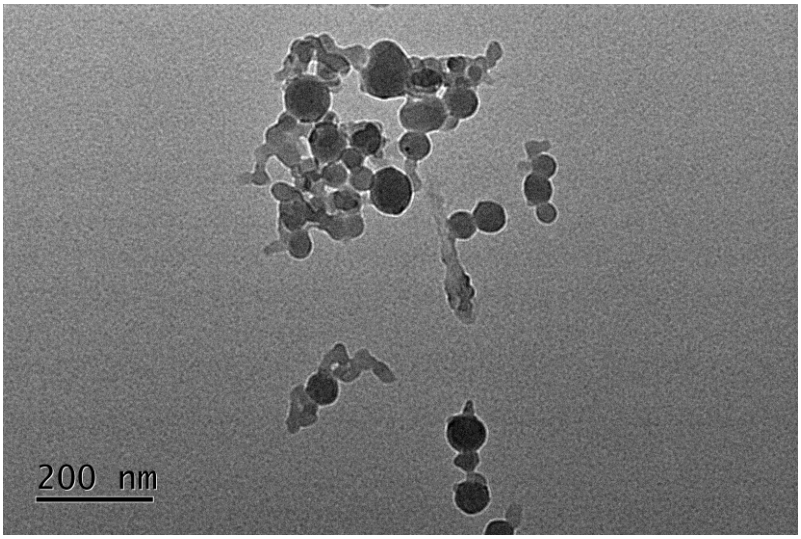

Fig. S10 TEM image of Au_{10}NC-PAH (1.6 μM).

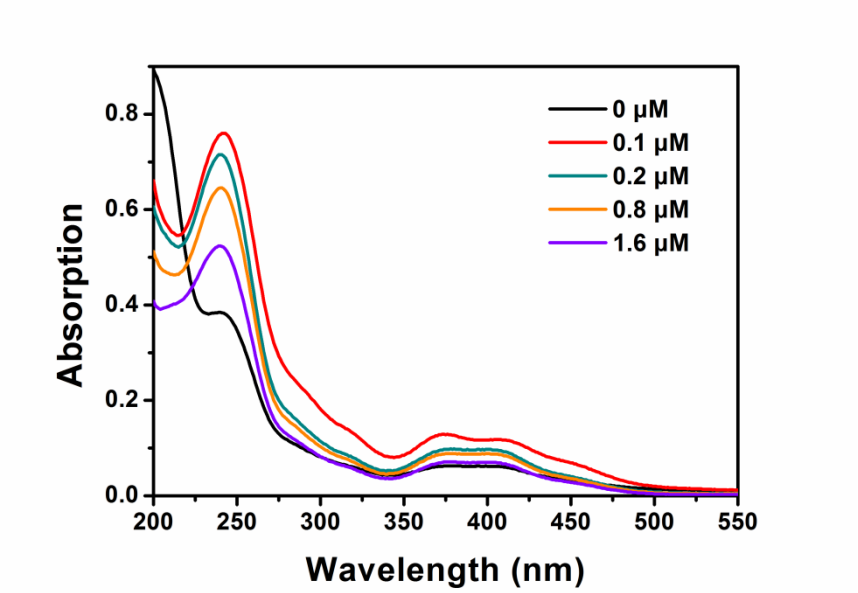

Fig. S11 Absorbance of Au_{10}NC-PAH with different PAH concentrations.

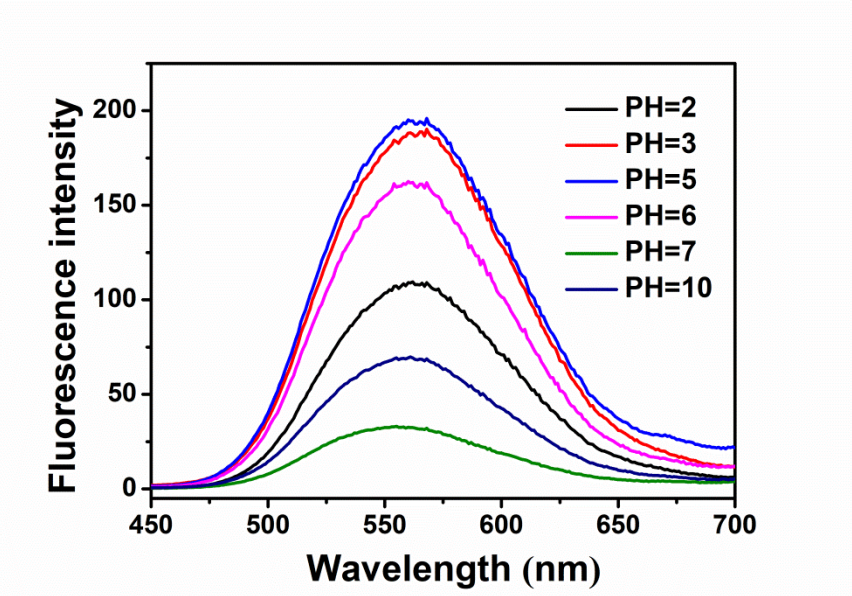

Fig. S12 Fluorescence emission of Au_{10}NC-PAH (0.2 μM) in aqueous solution at different pH.

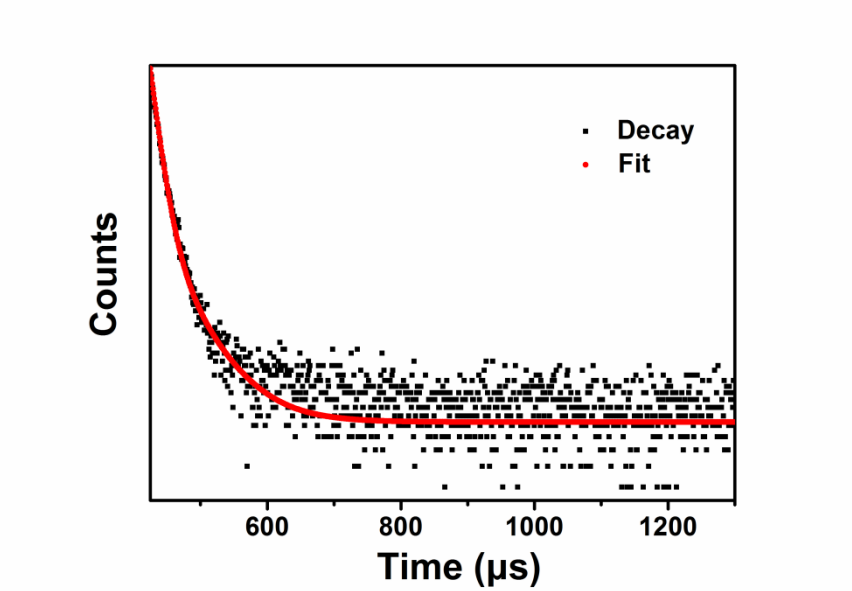

Fig. S13 Photoluminescence decays of Au_{10}NCs aqueous solution.

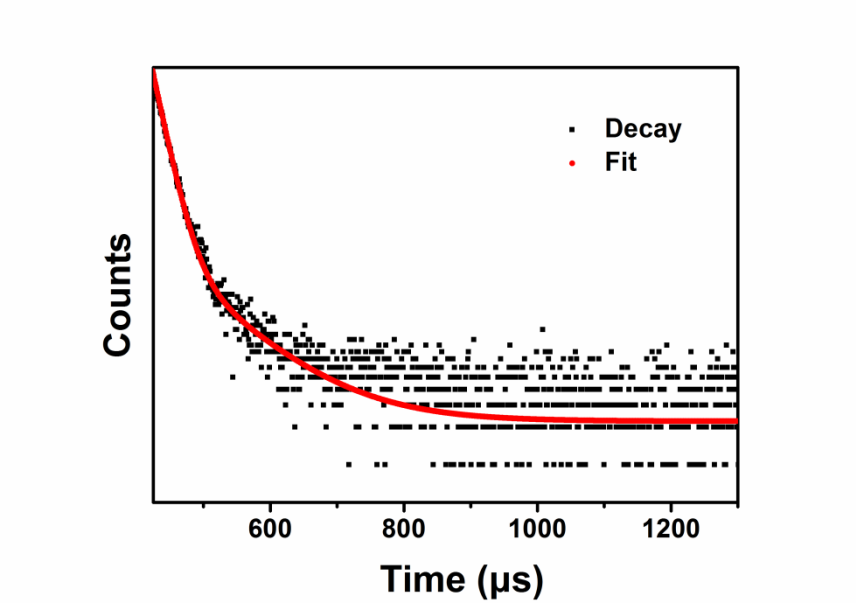

Fig. S14 Photoluminescence decays of Au_{10}NC-PAH.

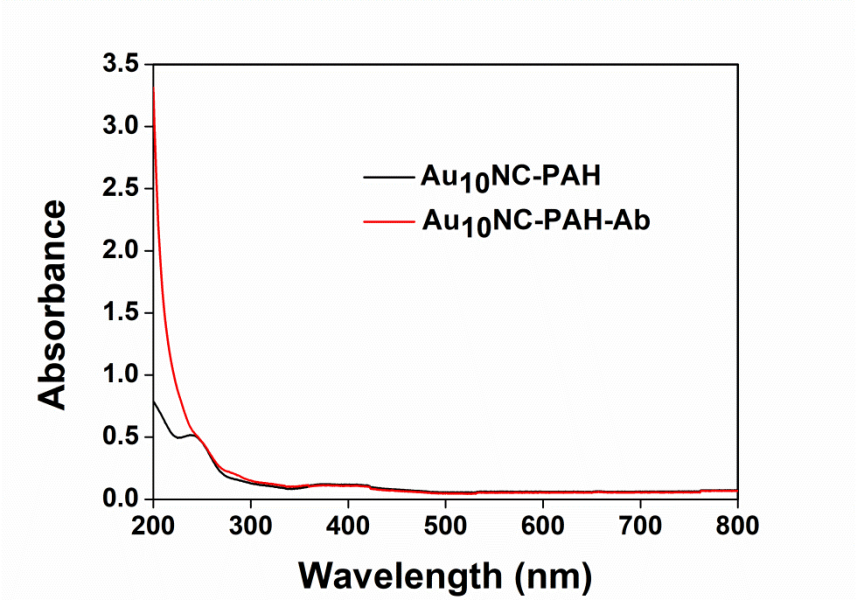

Fig. S15 UV-Vis absorbance spectra of Au_{10}NC-PAH (black line) and Au_{10}NC -PAH-Ab (red line).

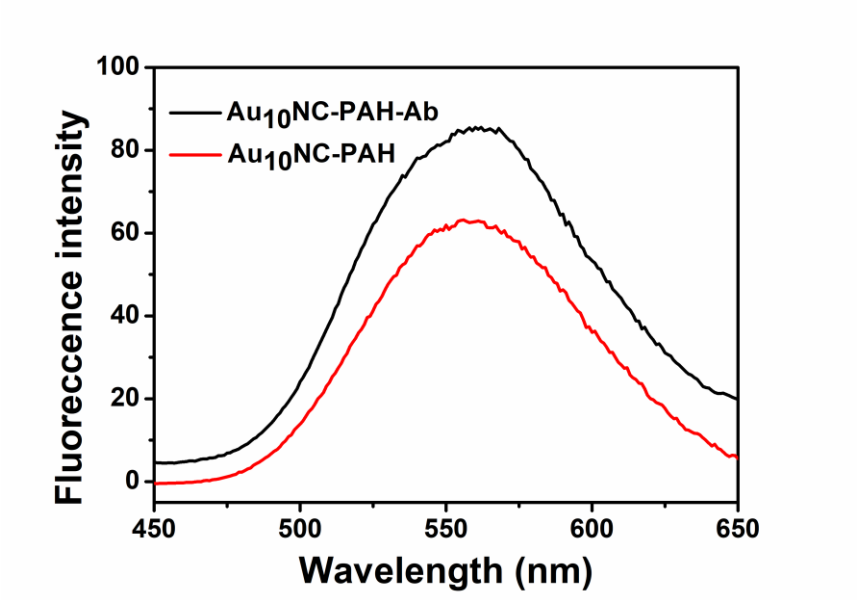

Fig. S16 Fluorescence emission of Au_{10}NC-PAH (red line) and Au_{10}NC-PAH-Ab (black line).

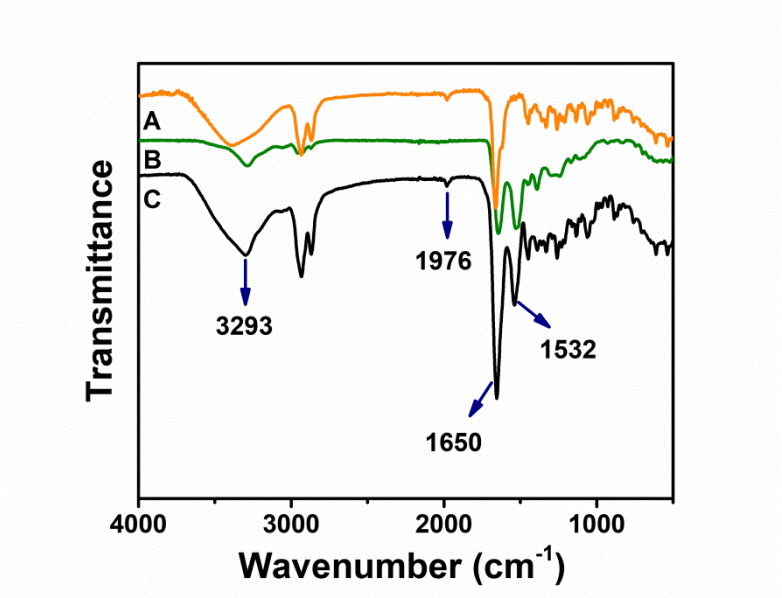

Fig. S17 FT-IR spectra of (A) Au_{10}NC-PAH, (B) Ab and (C) Au_{10}NC-PAH-Ab.

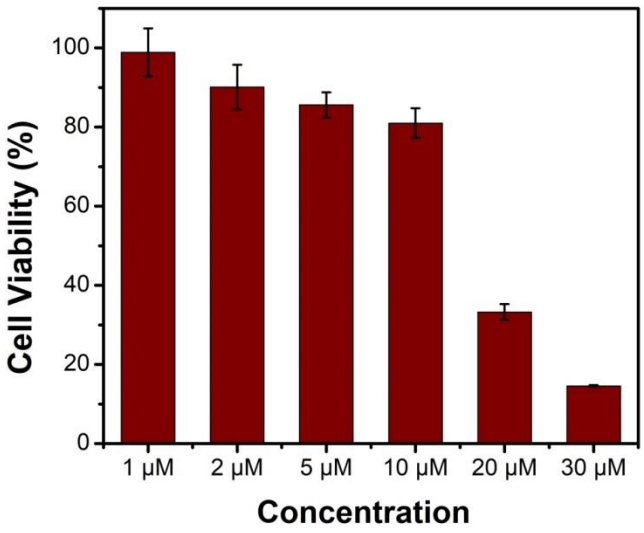

Fig. S18 Viability of NG108-15 cells incubated with different concentrations of Au_{10}NC-PAH-Ab for 24 h.

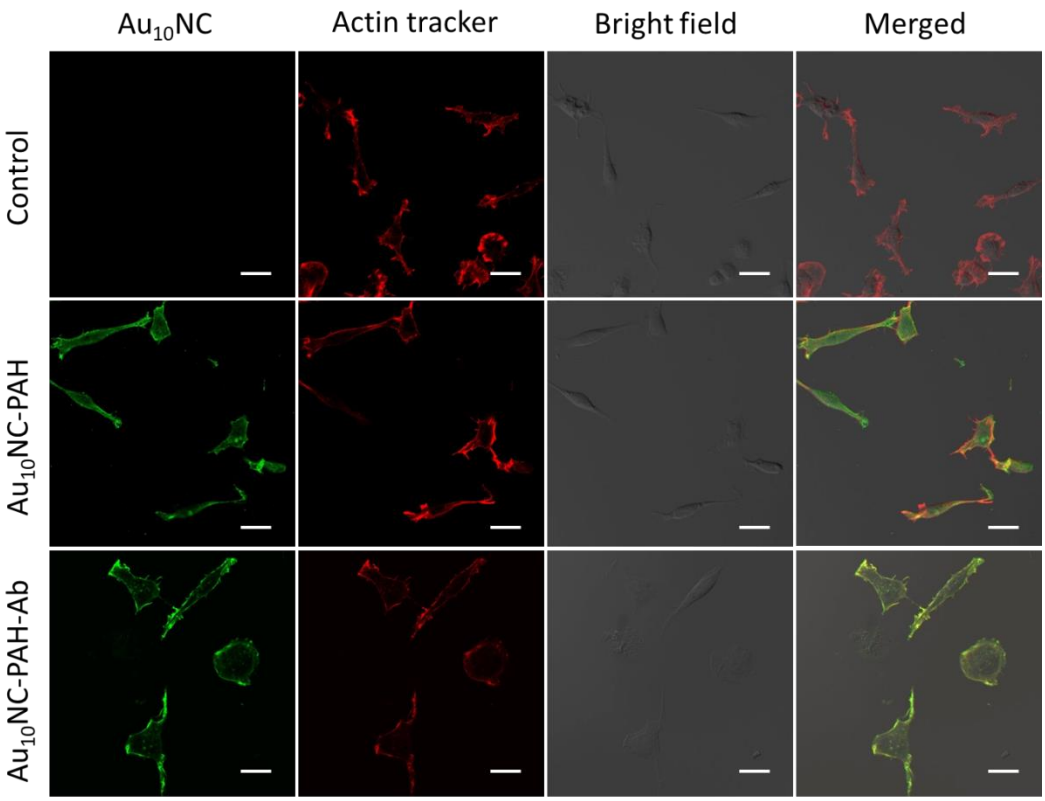

Fig. S19 Confocal images of HeLa cells incubated with Au_{10}NC-PAH and Au_{10}NC-PAH-Ab. Scale bars: 25 μm.

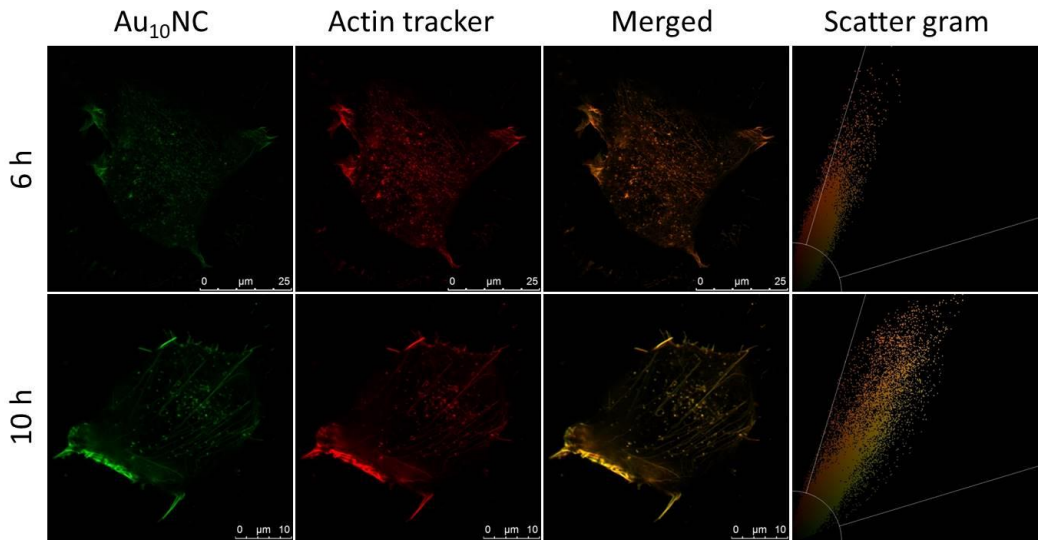

Fig. S20 High-resolution confocal images of NG108-15 cells incubated with Au_{10}NC-PAH-Ab for different time (Pearson's correlations of 6h and 10 h are 0.86, 0.92 respectively).

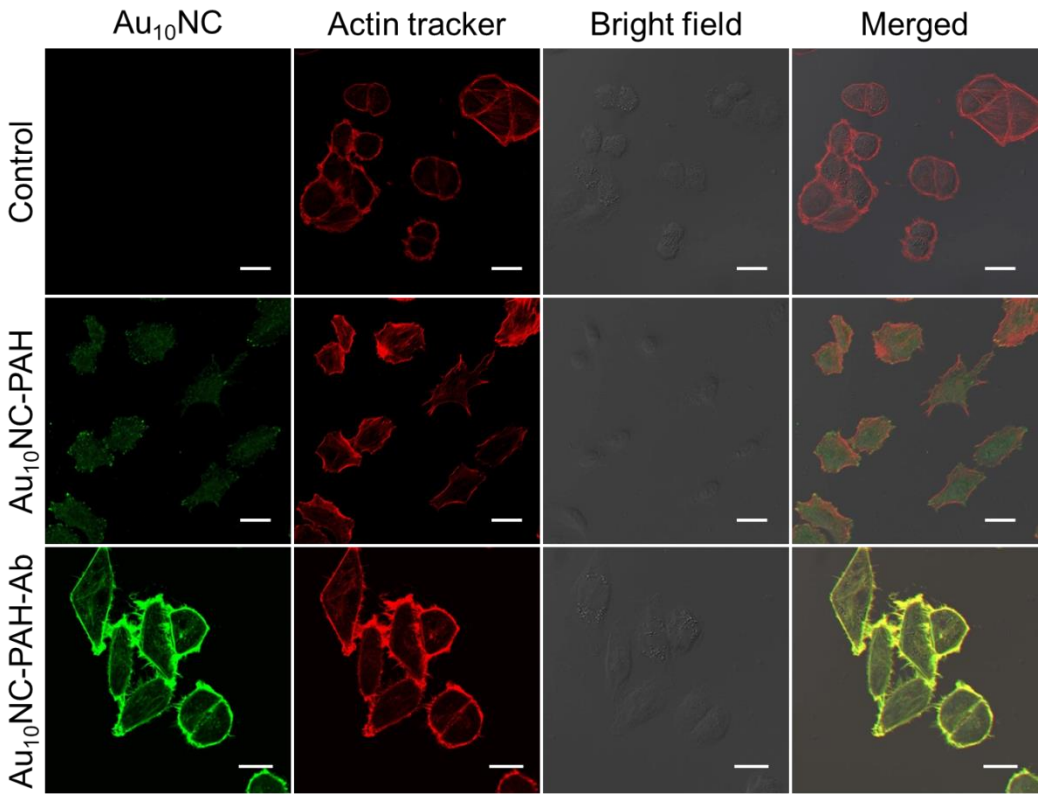

Fig. S21 Confocal images of HeLa cells incubated with Au_{10}NC-PAH and Au_{10}NC-PAH-Ab. Scale bars: 25 μm.

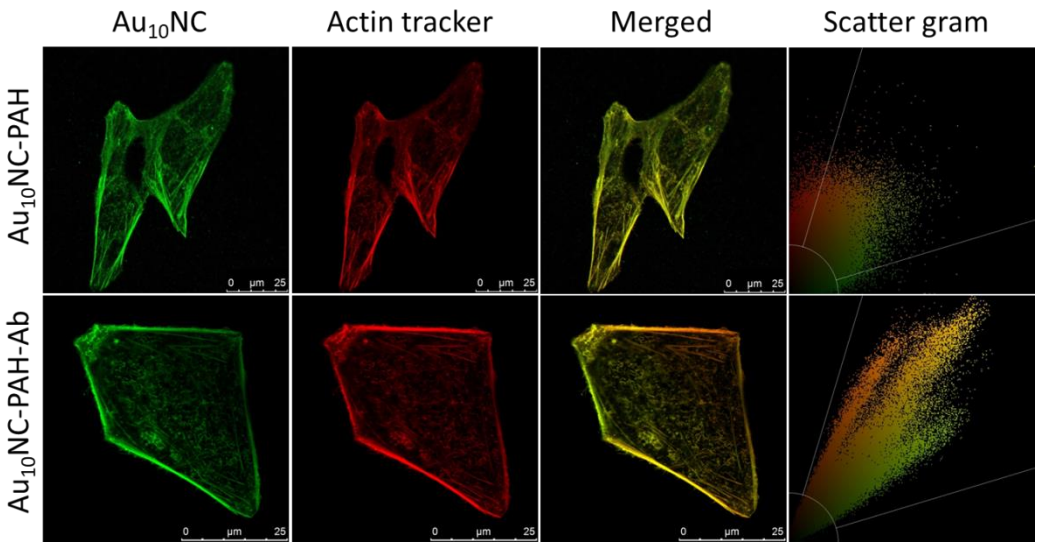

Fig. S22 High-resolution confocal images of HeLa cells incubated with Au_{10}NC-PAH (Pearson's correlation: 0.73, overlap coefficient: 0.74) and Au_{10}NC-PAH-Ab (Pearson's correlation: 0.94, overlap coefficient: 0.95).

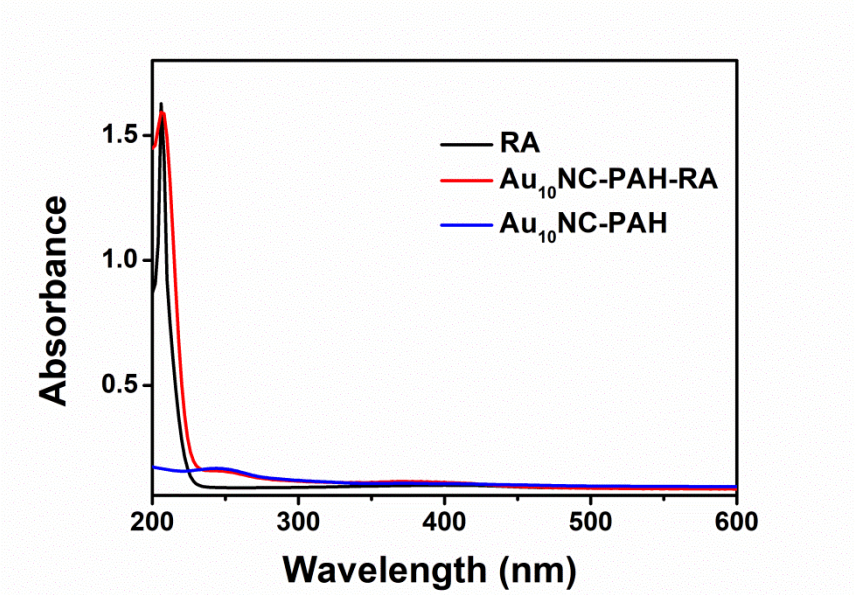

Fig. S23 UV-Vis absorbance spectra of RA (black line), Au_{10}NC-PAH-RA (red line) and Au_{10}NC-PAH (blue line).

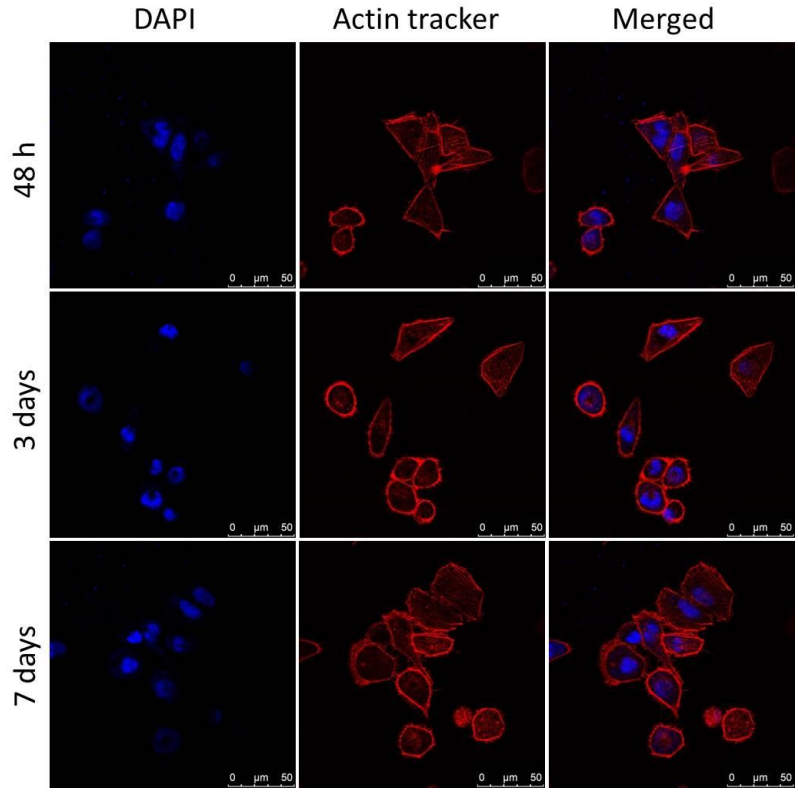

Fig. S24 Confocal images of HeLa cells incubated with 1 μM RA for different time.

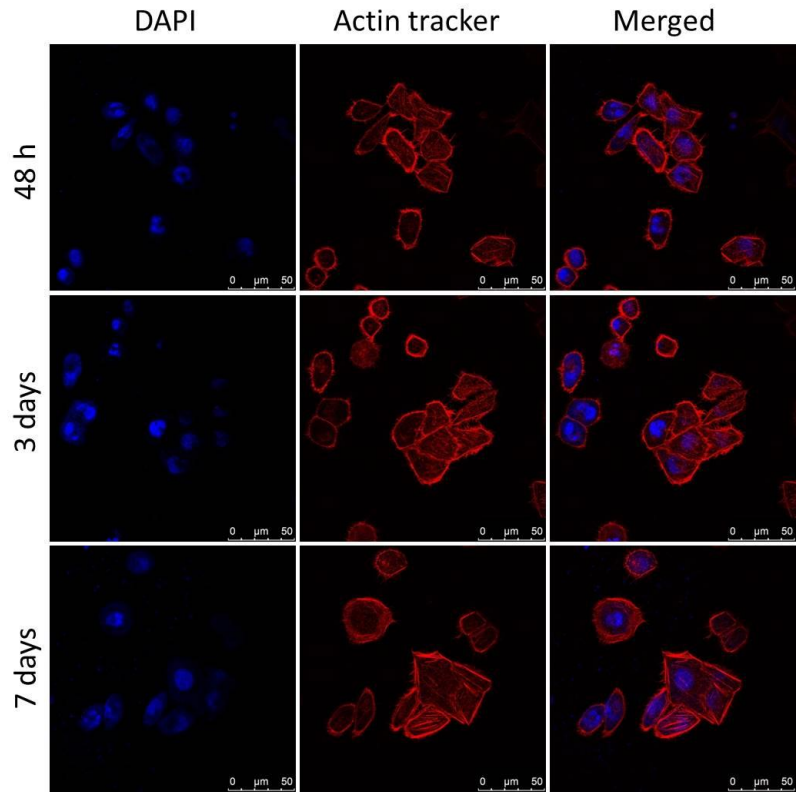

Fig. S25 Confocal images of HeLa cells incubated with Au_{10}NC-PAH-RA (1 μM RA equivalent concentration) for different time.

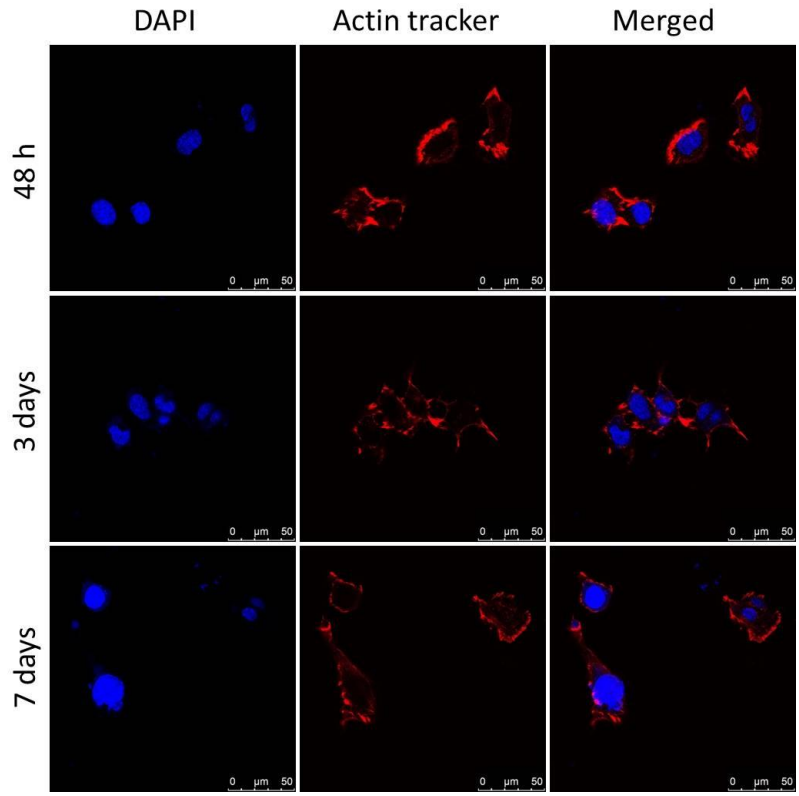

Fig. S26 Confocal images of NG108-15 cells incubated as control for different time.

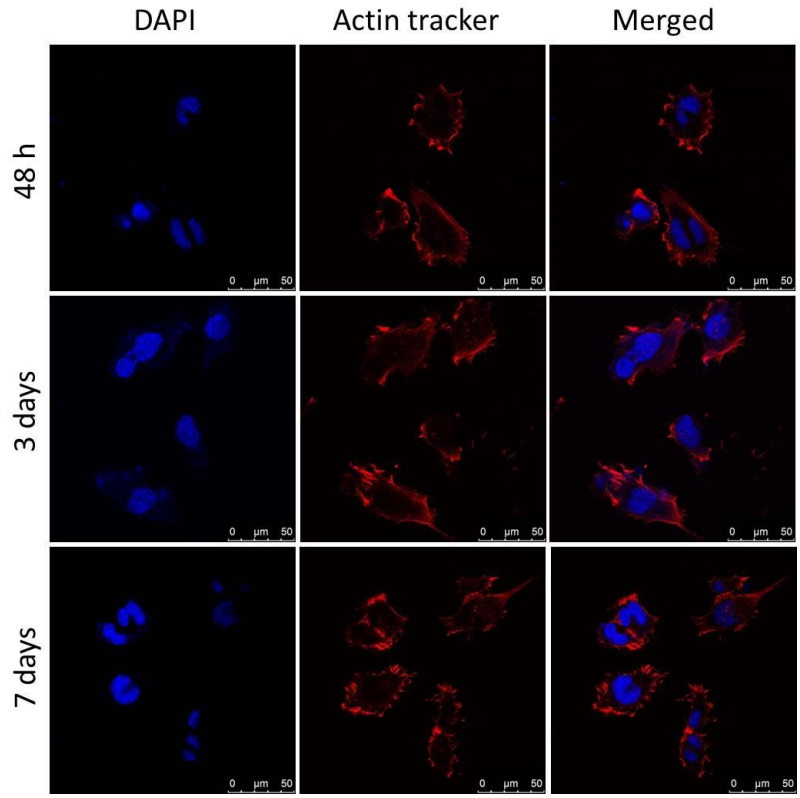

Fig. S27 Confocal images of NG108-15 cells incubated with Au_{10}NC-PAH (containing 1.15 μM Au_{10}NCs) for different time.

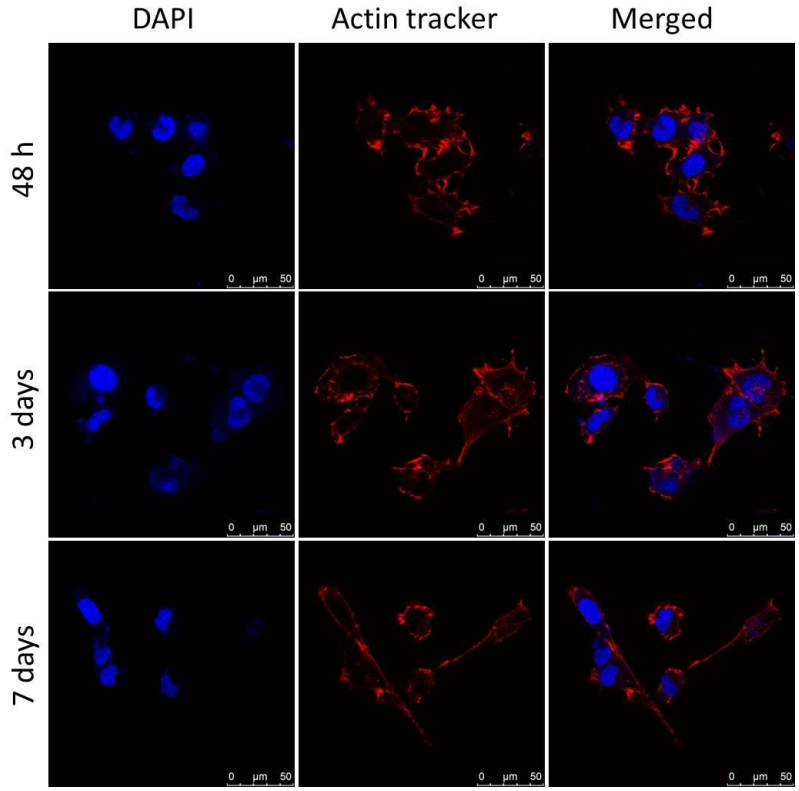

Fig. S28 Confocal images of NG108-15 cells incubated with 1 μM free RA for different time.

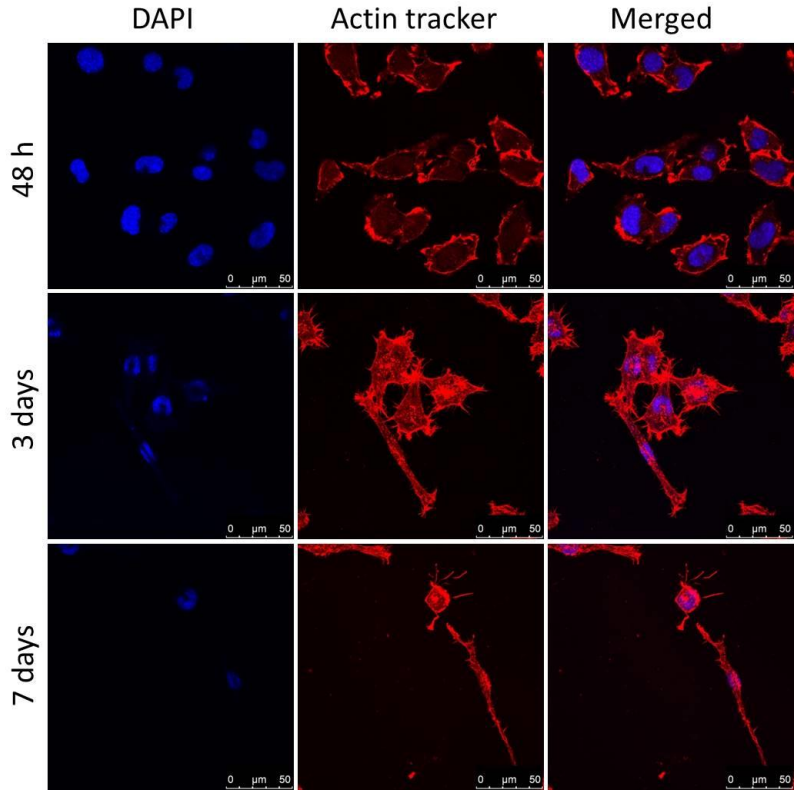

Fig. S29 Confocal images of NG108-15 cells incubated with Au_{10}NC-PAH-RA (0.5

μM RA equivalent concentration) for different time.

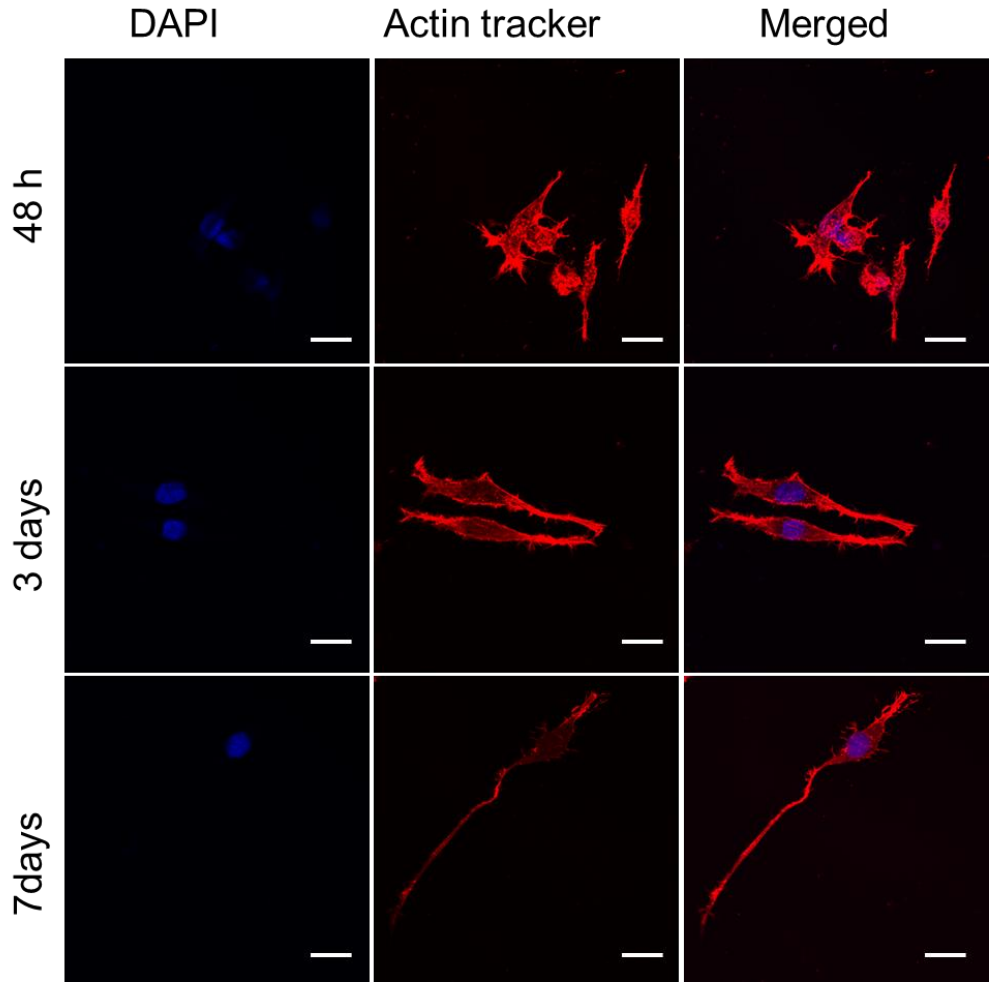

Fig. S30 Confocal images of NG108-15 cells cultured with Au_{10}NC-PAH-RA (1 μM RA equivalent concentration) for different time. Bars: 25 μm.

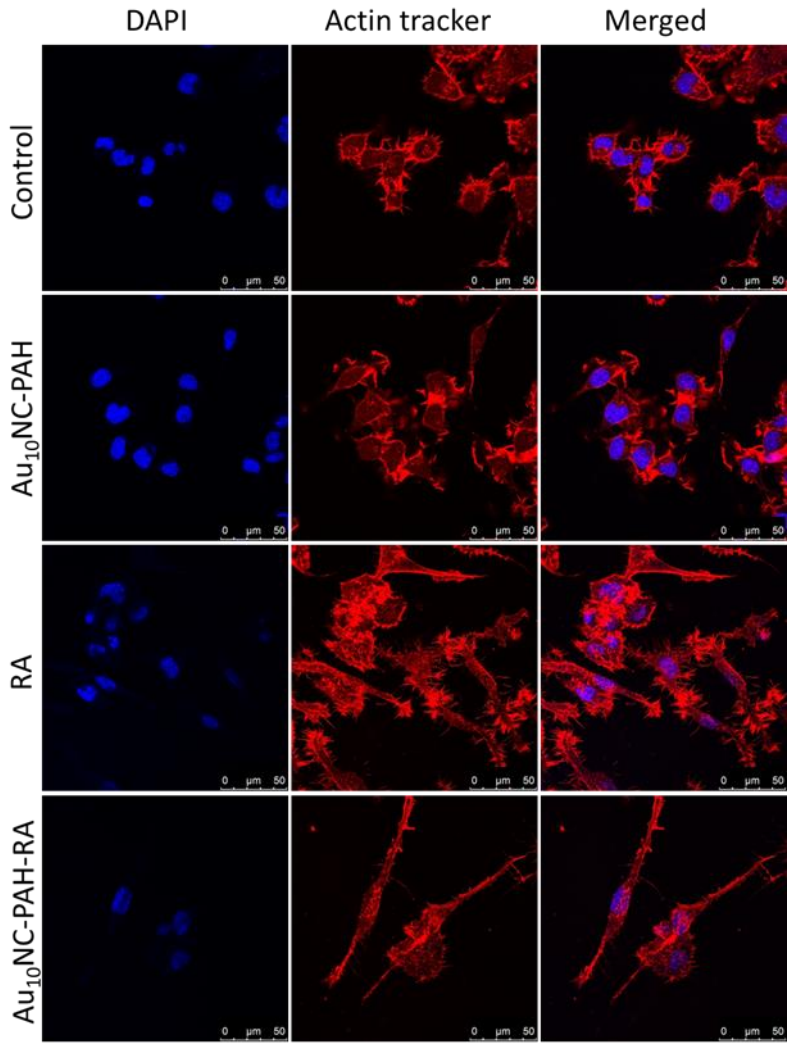

Fig. S31 Supplementary confocal images of NG108-15 cells incubated with RA loaded Au10NC-PAH assemblies for 7 days (Red, actin; blue, nucleus).

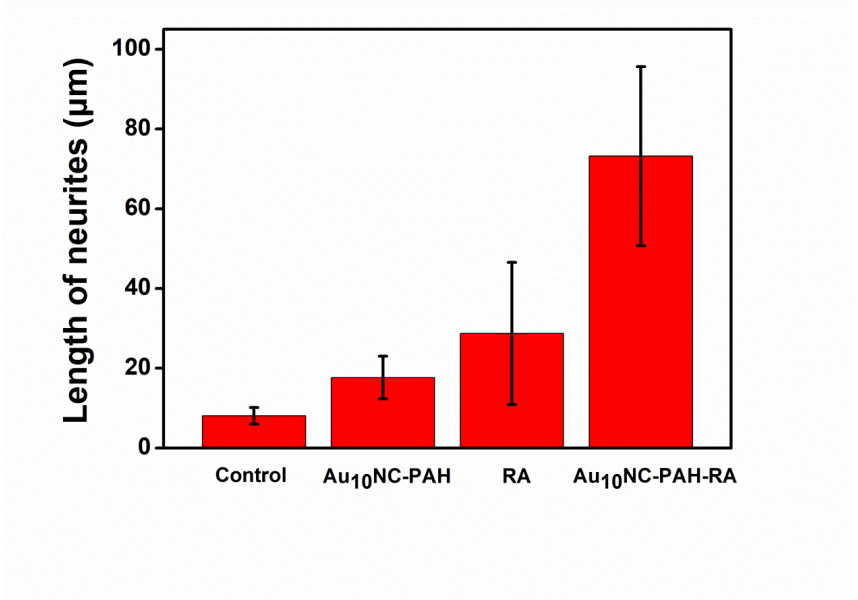

Fig. S32 Neurites lengths of NG108-15 cells with different treatments.

Table S1. Crystal data and structure refinement for Au_{10}NCs.

CCDC number	1995917
Empirical formula	$C_{214}H_{282}Au_{10}O_{22}S_2$
Formula weight	5240.16
Temperature/K	150.00(10)
Crystal system	orthorhombic
Space group	$P2_12_12$
a/Å	19.6562(4)
b/Å	28.6975(5)
c/Å	21.2232(4)
α/°	90
β/°	90
γ/°	90
Volume/Å^3	11971.7(4)
Z	2
ρ_{calc} g/cm^3	1.454
μ/mm^{-1}	6.172
F(000)	5128.0
Crystal size/mm^3	0.3 × 0.2 × 0.05
Radiation	MoKα (λ = 0.71073)
2Θ range for data collection/°	3.838 to 58.182
Index ranges	$-26 \le h \le 25$, $-38 \le k \le 39$, $-28 \le l \le 28$
Reflections collected	319546
Independent reflections	30031 [R_{int} = 0.1049, R_{sigma} = 0.0761]
Data/restraints/parameters	30031/187/1130
Goodness-of-fit on F^2	1.093
Final R indexes [I>=2σ (I)]	R_1 = 0.0460, wR_2 = 0.1064
Final R indexes [all data]	R_1 = 0.0760, wR_2 = 0.1138
Largest diff. peak/hole / e Å^{-3}	0.97/-0.99
Flack parameter	0.156(8)

$R1 = \sum||Fo|-|Fc||/\sum|Fo|$. $wR2 = [\sum w(Fo2 - Fc2)2/\sum w(Fo2)2]^{1/2}$

Table S2. Au–Au and Au–C bond length in Au_{10}NCs.

Atom	Length/Å
Au1-Au2[1]	2.9417(6)
Au2-Au1[1]	2.9417(6)
Au2-Au2[1]	2.9168(8)
Au2-Au3	3.0193(6)
Au2-Au4	2.9121(6)
Au2-Au5	2.9692(6)
Au3-Au4	3.3007(7)
Au1-C3[1]	2.200(10)
Au1-C6	2.211(11)
Au1-C9[1]	2.250(13)
Au1-C28	2.257(10)
Au2-C7	1.996(12)
Au2-C28	1.992(12)
Au3-C1	2.023(12)
Au3-C3	1.990(12)
Au4-C1	2.196(12)
Au4-C2	1.963(13)
Au4-C27	2.216(12)
Au5-C2	2.216(11)
Au5-C7[1]	2.203(10)
Au5-C19	2.175(14)
Au5-C38[1]	2.220(11)
C3-Au1[1]	2.200(10)
C7-Au5[1]	2.203(10)
C9-Au1[1]	2.250(13)
C38-Au5[1]	2.220(11)

[1] *1-X,1-Y,+Z*

Table S3. Bond angles (°) for **Au_{10}NCs.**

Atom	Angle/°
C3[1]-Au1-Au2[1]	85.2(3)
C3[1]-Au1-C6	160.4(4)
C3[1]-Au1-C9[1]	32.1(4)
C3[1]-Au1-C28	164.9(4)
C6-Au1-Au2[1]	108.6(3)
C6-Au1-C9[1]	134.5(4)
C6-Au1-C28	32.4(4)
C9[1]-Au1-Au2[1]	116.4(3)
C9[1]-Au1-C28	162.0(4)
C28-Au1-Au2[1]	79.8(3)
Au1[1]-Au2-Au3	72.252(15)
Au1[1]-Au2-Au5	144.950(19)
Au2[1]-Au2-Au1[1]	75.131(14)
Au2[1]-Au2-Au3	146.585(15)
Au2[1]-Au2-Au5	70.881(16)
Au4-Au2-Au1[1]	139.74(2)
Au4-Au2-Au2[1]	145.05(2)
Au4-Au2-Au3	67.597(15)
Au4-Au2-Au5	74.305(16)
Au5-Au2-Au3	139.243(19)
C7-Au2-Au1[1]	86.2(3)
C7-Au2-Au2[1]	91.8(3)
C7-Au2-Au3	93.1(3)
C7-Au2-Au4	92.9(3)
C7-Au2-Au5	103.0(3)
C28-Au2-Au1[1]	90.7(3)
C28-Au2-Au2[1]	84.6(3)
C28-Au2-Au3	88.7(3)
C28-Au2-Au4	91.3(3)
C28-Au2-Au5	78.0(3)
C28-Au2-C7	175.8(4)
Au2-Au3-Au4	54.655(13)
C1-Au3-Au2	94.4(3)
C1-Au3-Au4	40.5(3)
C3-Au3-Au2	86.8(3)
C3-Au3-Au4	141.1(3)
C3-Au3-C1	177.2(5)
Au2-Au4-Au3	57.748(14)
C1-Au4-Au2	93.8(3)
C1-Au4-Au3	36.7(3)
C1-Au4-C27	31.2(4)
C2-Au4-Au2	87.1(3)
C2-Au4-Au3	143.9(3)
C2-Au4-C1	178.7(5)
C2-Au4-C27	148.2(4)
C27-Au4-Au2	124.3(3)
C27-Au4-Au3	67.9(3)

C2-Au5-Au2	81.3(3)
C2-Au5-C38[1]	157.7(5)
C7[1]-Au5-Au2	86.5(3)
C7[1]-Au5-C2	167.8(5)
C7[1]-Au5-C38[1]	33.2(4)
C19-Au5-Au2	113.4(4)
C19-Au5-C2	32.2(5)
C19-Au5-C7[1]	159.9(5)
C19-Au5-C38[1]	128.6(5)
C38[1]-Au5-Au2	117.1(3)
Au3-C1-Au4	102.8(5)
C27-C1-Au3	178.0(11)
C27-C1-Au4	75.3(8)
Au4-C2-Au5	116.3(5)
C19-C2-Au4	171.0(11)
C19-C2-Au5	72.0(8)
Au3-C3-Au1[1]	114.0(6)
C9-C3-Au1[1]	76.2(8)
C9-C3-Au3	169.8(10)
C8-C6-Au1	123.4(8)
C28-C6-Au1	75.8(7)
Au2-C7-Au5[1]	108.7(5)
C38-C7-Au2	171.3(10)
C38-C7-Au5[1]	74.1(7)
C3-C9-Au1[1]	71.7(8)
C11-C9-Au1[1]	119.2(8)
C2-C19-Au5	75.8(9)
C70-C19-Au5	129.4(9)
C1-C27-Au4	73.5(8)
C84-C27-Au4	116.3(9)
Au2-C28-Au1	114.3(5)
C6-C28-Au1	71.8(7)
C6-C28-Au2	172.8(9)
C7-C38-Au5[1]	72.7(7)
C25-C38-Au5[1]	121.7(8)

[1] *1-X,1-Y,+Z*

References

1 CrysAlisPro, Version 1.171.36.31, Agilent technologies, 2012.

2 G. M. Sheldrick, *Acta Crystallogr., Sect. A.* 2008, **64**, 112-122.

3 O. V. Dolomanov, L. J. Bourhis, R. J. Gildea, J. A. K. Howard, H. Puschmann, *J. Appl. Crystallogr.* 2009, **42**, 339.

4 G. M. Sheldrick, *Acta crystallogr. C.* 2015, **71**, 3-8.